Accurate Measurement of the 12.6 GHz "Clock" Transition in Trapped $^{171}Yb^{+}$ Ions

Peter T. H. Fisk, Matthew J. Sellars, Malcolm A. Lawn, and Colin Coles

Abstract—**We have measured the frequency of the $^{171}Yb^{+}$ 12.6 GHz $M_F = 0 \rightarrow 0$ ground state hyperfine "clock" transition in buffer gas-cooled ion clouds confined in two similar, but not identical, linear Paul traps. After correction for the known differences between the two ion traps, including significantly different second-order Doppler shifts, the frequencies agree within an uncertainty of less than 2 parts in 10^{13}. Our best value, based on an analytic model for the second-order Doppler shift, for the frequency of the clock transition of an isolated ion at zero temperature, velocity, electric field and magnetic field, is 12642812118.466 ± 0.002 Hz.**

I. Introduction

Investigations of the suitability as microwave frequency standards of ground-state hyperfine transitions ("clock" transitions) in clouds of buffer gas-cooled $^{199}Hg^{+}$ and $^{171}Yb^{+}$ ions confined in radio frequency (RF) Paul traps have raised questions concerning the frequency offsets arising from the Paul trap environment [1]–[9]. Some of these offsets can be relatively large, and also difficult to quantify, and may therefore limit the accuracy of a trapped-ion frequency standard. For example, the quadratic Stark shift of the 12.6 GHz ground state hyperfine transition of buffer gas-cooled $^{171}Yb^{+}$ ions due to the confining RF fields in a hyperbolic Paul trap has been measured as -7 parts in 10^{13} [1], with an uncertainty of approximately 50%. In the same system, the magnitude of the second-order Doppler shift is greater than 1 part in 10^{12}, depending on the operating conditions of the trap, again with an uncertainty of approximately 50%. Analogous measurements [10] on buffer gas-cooled $^{199}Hg^{+}$ ions in a hyperbolic Paul trap have indicated a limiting accuracy of 2.5 parts in 10^{13}.

In the case of a hyperbolic Paul trap, the node of the RF electric field, which is the bottom of the confining pseudo-potential well, is a geometric point. Due to the mutual Coulomb repulsion of the ions, an ion cloud must necessarily extend into the region where the confining RF electric field is non-zero. This results in the observed significant quadratic Stark shifts, and induces micro-motion of the ions at the RF frequency which contributes to the second-order Doppler shift as well as RF heating of the ion cloud. The linear ion trap configuration is advantageous [11] for frequency standards purposes because the node of the confining RF field is a line. This results in a substantially smaller influence of the confining RF fields on a cloud of a given number of ions than in a hyperbolic trap.

In both the hyperbolic and linear trap types the magnitudes of the second-order Doppler shift and the quadratic Stark shift depend on the physical properties of the ion cloud, which are difficult to measure directly. The calculation of the resulting frequency offsets must, therefore, rely on a model of the ion cloud which is based on measurable parameters, such as the trap dimensions, the temperature of the ion cloud and the frequencies (secular frequencies) at which the ions oscillate in the confining pseudo-potential well. The validity of such a model may ultimately prove to be a limiting factor for the accuracy of a trapped ion frequency standard.

We have previously reported [5], [6] some aspects of the performance of a prototype frequency standard (IT-1) based on the 12.6 GHz ground state hyperfine "clock" transition in $^{171}Yb^{+}$ ions confined in a linear Paul trap. More recently, we constructed a second prototype standard (IT-2), similar to IT-1 but with significant improvements in magnetic shielding and optical detection efficiency. A comparison [12] of the measured clock transition frequencies of the two traps under conditions where they contain different numbers of ions, and consequently ion clouds of different sizes, provided an early test of a model which gives values for the differing second-order Doppler shifts in the two traps. In the current paper we present the results of a more extensive investigation of the validity of this model. We also present the results of several measurements, over a period of more than 1 year, of the absolute frequency of the $^{171}Yb^{+}$ 12.6 GHz "clock" transition.

II. Experimental

The electrode structure of the ion trap systems IT-1 and IT-2 (Fig. 1) has been described previously [5], [6], [12]–[14]. Since the publication of [12] the arrangement of the vacuum system and magnetic shielding of IT-1 has been upgraded to be equivalent to that of IT-2, and is shown in Fig. 2. The important features of both ion trap systems are described here.

A. Magnetic Shielding

The ion trap systems have five layers of shielding consisting of an inner layer of silicon steel, surrounded by

Manuscript received September 6, 1995; accepted August 2, 1996.

The authors are with National Measurement Laboratory, CSIRO Telecommunications and Industrial Physics, P.O. Box 218 Lindfield NSW 2070, Sydney, Australia.

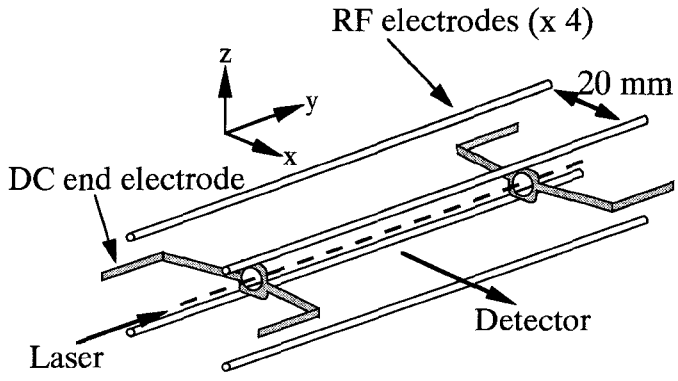

Fig. 1. Schematic electrode structure of the linear ion traps IT-1 and IT-2. In this paper we refer to motion in the x-z plane as transverse, and motion in the y direction as longitudinal. The diameter of the RF electrodes is 2.3 mm.

two layers of Co-Netic magnetic shielding material, surrounded in turn by another layer of silicon steel. The entire apparatus, including the photomultiplier housing, turbo-molecular pump and electrical feed-throughs, is surrounded by an outer layer of silicon steel, to form a box with edge dimensions 1.1 m × 1.4 m × 1.6 m (h). The total shielding factor of this system was measured as approximately 250.

B. Optical Delivery

The 369 nm laser light used to probe the $^{171}Yb^{+}$ optical resonance transition was delivered to both systems via a 200 μm core diameter multi-mode optical fiber. This allowed the ion traps to be located in a different room from the laser system (a frequency doubled titanium:sapphire laser pumped by an argon ion laser), and its associated major magnetic influence. Approximately 50 μW of laser light entered the ion traps.

The loading, operation, and microwave interrogation sequence of both systems were essentially the same as described previously [5], [6], and the operational parameters are shown in Table I. The 12.6 GHz microwave signal for each ion trap was synthesized separately (Fig. 3) from a common source [5], [6], based on a sapphire-loaded superconducting resonator [15]. For the absolute clock frequency measurements described in this paper, the microwave $\pi/2$ pulse duration was 400 ms, with the pulse centers separated by 25 s, yielding Ramsey fringes with a period of 40 mHz. For the frequency stability measurements, the interval between the $\pi/2$ pulses was set to 50 s. The phase transients associated with the microwave pulses were investigated and, for the mode of operation of the frequency synthesis system used to generate the data presented in this paper, were found to contribute a frequency offset of less than 0.1 mHz, which is presently negligible.

The laser system, which generates the 369.4 nm radiation used to probe the populations of the $^{171}Yb^{+}$ ground state hyperfine levels following the microwave interrogation pulse sequence, is common to both ion trap systems. The laser radiation is not expected to produce any long-

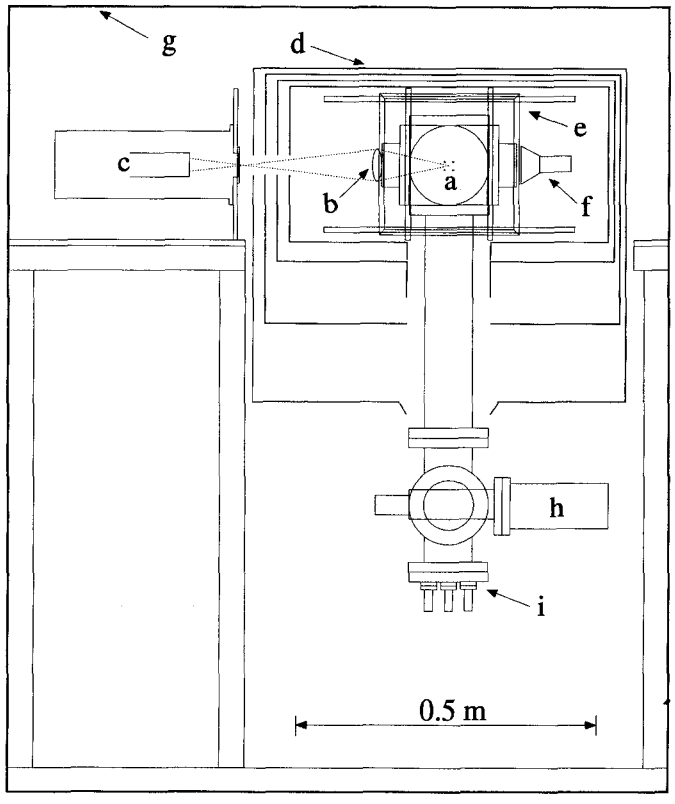

Fig. 2. Schematic diagram of the ion trap systems IT-1 and IT-2. a) Trap RF electrodes, b) fluorescence focussing lens, c) photomultiplier tube, d) magnetic shielding (4 layers, see text), e) Helmholtz coils, f) microwave horn, g) outer magnetic shield, h) turbo-molecular pump, i) electrical vacuum feedthroughs.

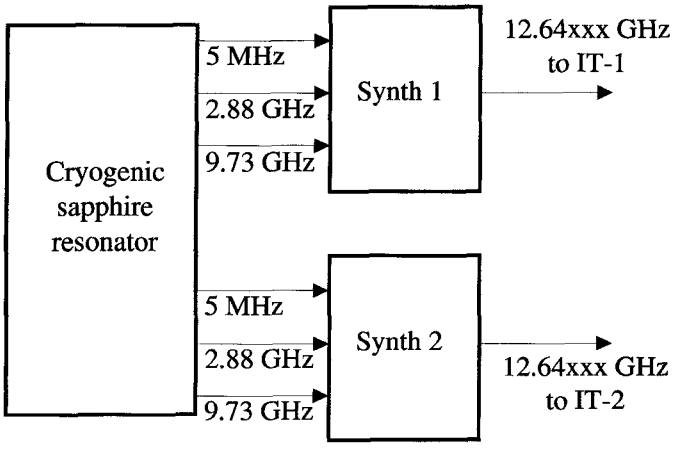

Fig. 3. Schematic diagram of the system used to generate the microwave interrogation signals for the two ion traps. Both 12.6 GHz signals were gated simultaneously to generate the Ramsey interrogation pulse sequence.

TABLE I

TYPICAL OPERATIONAL PARAMETERS APPLIED TO THE ION TRAPS FOR THE MEASUREMENTS DESCRIBED IN THIS PAPER. FOR SOME OF THE MEASUREMENTS DESCRIBED IN THIS PAPER, THE RF AMPLITUDES, END-ELECTRODE VOLTAGES, AND HELIUM PRESSURES WERE VARIED. THE UNCERTAINTY IN THE HELIUM PRESSURE IS THE VARIATION OBSERVED BETWEEN THE READINGS OF TWO INDEPENDENT GAUGE HEADS AND GAUGE CONTROLLERS CONNECTED TO A SINGLE VACUUM SYSTEM. THE VALUE QUOTED IS CORRECTED FOR RELATIVE GAUGE SENSITIVITY TO He USING THE CALIBRATION FACTOR GIVEN BY THE GAUGE MANUFACTURER.

	IT-1	IT-2
RF electrode separation	20 mm	20 mm
RF electrode diameter	2.3 mm	2.3 mm
End electrode separation	60 mm	60 mm
RF frequency	500 kHz	510 kHz
RF amplitude	$287 \pm 3V_{p-p}$	$280 \pm 3V_{p-p}$
End electrode voltage	10.0 V (stability ± 0.001 V)	10.0 V (stability ± 0.001 V)
He pressure	$1.2 \pm 0.6 \times 10^{-4}$ Pa	$1.7 \pm 0.6 \times 10^{-4}$ Pa

term offsets, correlated or otherwise, in the clock frequencies of the two systems, since the laser light is blocked during the microwave interrogation sequence [5], [6]. The laser power is actively stabilised, with a residual fluctuation of approximately 1% .

Isolation of IT-1 from the microwave interrogation radiation applied to IT-2, and vice-versa, was better than 50 dB. At the present level of precision, the effects of microwave cross-talk between the two systems are too small to be measured. There are also a number of sidebands on the 12.6 GHz signal, due to the mixing scheme used in its generation [5], [6]. The maximum shift in the measured clock frequency induced by these sidebands was calculated as 2 parts in 10^{15}, which is currently negligible.

III. RESULTS

The results of measurements made on the two ion traps are shown in Table II.

The frequency of the 12.6 GHz $^{171}Yb^{+}$ $M_F = 0 \rightarrow 0$ hyperfine resonance in each ion trap was measured by locking [5], [6] the two 12.6 GHz signals to the Ramsey fringe pattern from each ion trap. The cycle time of the experiment was such that one frequency measurement was made on both traps every 72 s. During each measurement cycle, the Larmor frequency in each trap was obtained by measuring the frequency separation of the $M_F = 0 \rightarrow 0$ and $M_F = 0 \rightarrow -1$ Zeeman components of the 12.6 GHz hyperfine transition [5], [6]. The Larmor frequency in each ion trap varied by less than 80 Hz during the period of the measurement, and the results for both the Larmor frequency and the clock frequency presented in Table II are averaged over this period.

The longitudinal and transverse secular frequencies were measured from the microwave excitation spectra from each trap, an example of which is shown in Fig. 4. The different ratios of longitudinal to transverse secular frequency in the two traps are not yet understood but are assumed to be associated with the supposedly minor differences in the shape of the end electrodes fitted to the two traps.

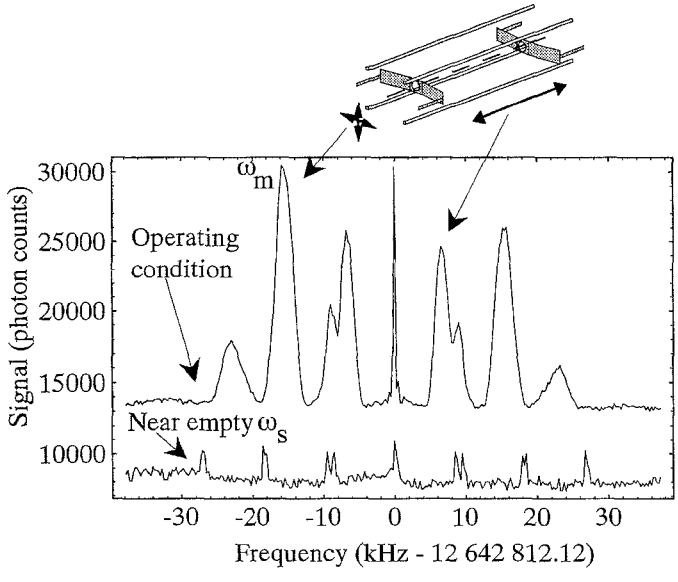

Fig. 4. Sideband structure on the 12.6 GHz clock transition in IT-2 due to longitudinal and transverse motion of the ions. The peaks due to the transverse secular motion with the trap loaded to a typical operating level, and near-empty, are labelled ω_m and ω_s, respectively.

The stability, characterized by the Allan deviation $\sigma_y(\tau)$, of the 12.6 GHz $^{171}Yb^{+}$ clock transition in IT-2 with respect to the hydrogen maser NML-Maser 2 is shown in Fig. 5. For integrating times between 114 s and 1000 s, the system exhibits a white noise-limited performance $\sigma_y(\tau) = 6 \times 10^{-14}\tau^{-1/2}$. Beyond 1000 s the measured performance is probably limited by the hydrogen maser.

Inspection of the Allan deviation of IT-2 with respect to the sapphire resonator-based local oscillator (LO) (Fig. 6) indicates that the hydrogen maser NML-Maser 2 contributes significantly to the Allan deviation shown in Fig. 5, and for averaging times less than 300 s, the performance of IT-2 is probably better than or equal to $\sigma_y(\tau) = 4.7 \times 10^{-14}\tau^{-1/2}$.

The expected performance of the system is given by [16]

$$\sigma_y(\tau) = \frac{\delta f}{\pi f_0}\left(\frac{N}{S}\right)\sqrt{\frac{T_c}{\tau}} \qquad (1)$$

TABLE II

MEASURED TRAP PARAMETERS CORRESPONDING TO THE CONDITIONS LISTED IN TABLE I. THE ION CLOUD LENGTH WAS MEASURED USING A UV-SENSITIVE CCD CAMERA, AND THE ION CLOUD TEMPERATURE WAS CALCULATED FROM THE MEASURED DOPPLER WIDTH OF THE OPTICAL TRANSITION [5], [6]. THE PRESSURE SHIFT DUE TO HELIUM WAS TAKEN FROM A PREVIOUS MEASUREMENT ON IT-1 [5], [6]. THE RAW CLOCK FREQUENCY IS THE UNCORRECTED FREQUENCY OF THE 12.6 GHZ $^{171}Yb^{+}$ $M_F = 0 \rightarrow 0$ GROUND-STATE HYPERFINE RESONANCE WITH RESPECT TO THE HYDROGEN MASER NML-MASER 2. NOTE 1: THESE ARE THE MEAN LARMOR FREQUENCIES OVER THE PERIOD OF MEASUREMENT (15 MEASUREMENT CYCLES), AND THE UNCERTAINTIES ARE BASED ON THE DIFFICULTY OF LOCATING THE CENTER OF THE ZEEMAN LINESHAPES DUE TO THEIR RESIDUAL ASYMMETRIES. NOTE 2: THESE ARE THE MEAN FREQUENCIES OVER THE PERIOD OF MEASUREMENT, AND THE UNCERTAINTIES REFLECT THE VARIATION DURING THIS TIME.

	IT-1	IT-2
Ion cloud length	not measured	0.024 m
Ion cloud temperature (longitudinal)	357 ± 30 K	371 ± 30 K
(transverse)	417±30 K	431 ± 30 K
Secular frequencies (trap loaded)		
longitudinal	4.5 ± 0.5 kHz	6.0 ± 0.5 kHz
transverse	16.6 ± 0.5 kHz	17.7 ± 0.5 kHz
Helium pressure shift	0.38 ± 0.15 mHz	0.58 ± 0.15 mHz
Larmor frequency (1)	70495 ± 5 Hz	71556 ± 5 Hz
Ramsey fringe amplitudes		
$M_F = 0 \rightarrow 0$ transition	17000 photon counts	37000 photon counts
$M_F = 0 \rightarrow -1$ transition	15000 photon counts	35000 photon counts
Laser scatter background	1000 photon counts	4000 photon counts
Raw clock frequency (2)	$12642812119.2529 \pm 0.0003$ Hz	$12642812119.2781 \pm 0.0003$ Hz

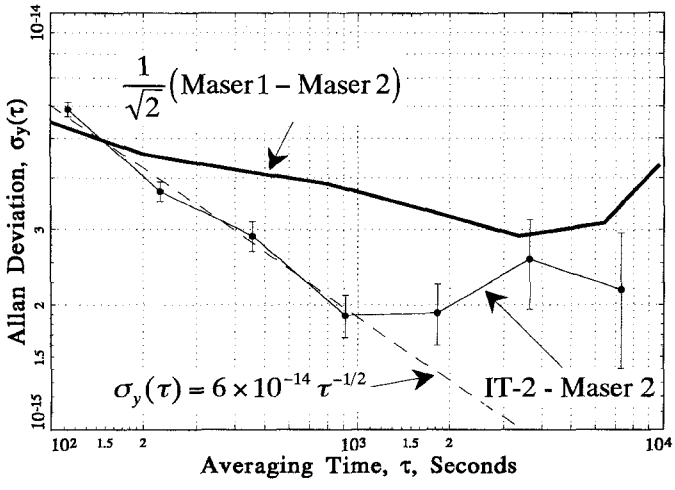

Fig. 5. Fractional Allan deviation of IT-2 with respect to NML-Maser 2. Routine monitoring of the two masers over the last 12 months has shown that the performance of Maser 2 is superior to that of Maser 1.

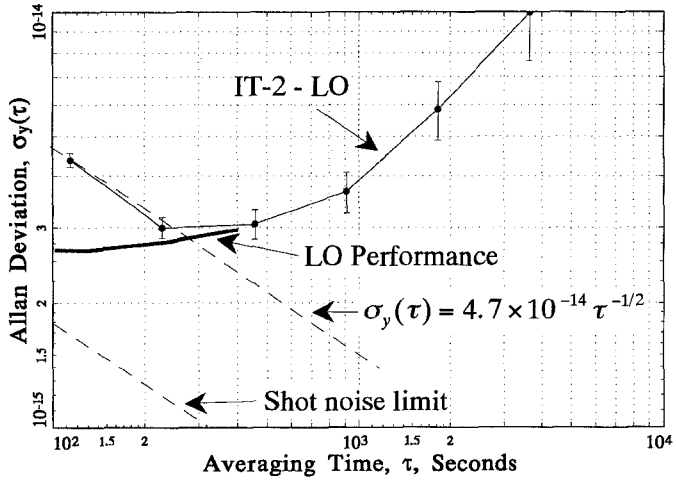

Fig. 6. Fractional Allan deviation of IT-2 with respect to the LO. The LO performance shown was measured with respect to a second cryogenic sapphire resonator-based source.

where δf is the width of the central Ramsey fringe, f_0 is the frequency of the clock transition, N/S is the single-measurement cycle noise-to-signal ratio and T_c is the measurement cycle time. If we assume that the noise in the signal arises solely from the shot noise associated with the process of measuring the probability of individual ions absorbing a microwave photon, (1) yields the performance limit of the frequency standard. For the conditions under which the data shown in Figs. 5 and 6 was obtained ($T_c = 114$ s), we calculate a performance limit $\sigma_y(\tau) = 1.8 \times 10^{-14}\tau^{-1/2}$, which is plotted on Fig. 6.

For $\tau = 114$ s, the in-quadrature combination of the shot noise contribution to the Allan deviation [calculated using (1)] and the measured LO performance, $\sigma_y(114\text{ s}) = 2.6 \times 10^{-15}$, predicts a limiting Allan deviation $\sigma_y(114\text{ s}) = 3.1 \times 10^{-15}$ for IT-2 with respect to the LO. This is to be compared with the observed value $\sigma_y(114\text{ s}) = 4.4 \times 10^{-15}$. The cause of the encouragingly small discrepancy between the limiting and observed Allan deviations at 114 s is not yet known precisely. However, any of a number of factors, such as short-term jitter in the frequency of the 369.5 nm laser, or frequency down-conversion of phase noise in the 12.6 GHz signal occurring over the time scales of the interrogating $\pi/2$ pulses, may be contributing.

IV. Accurate Determination of the Clock Frequency

We now calculate the frequency, referenced to TAI (International Atomic Time), of the 12.6 GHz $^{171}Yb^{+}$ $M_F = 0 \rightarrow 0$ ground state hyperfine transition in a stationary ion at zero magnetic field in a perfect vacuum. The calculated magnitudes of the shifts corresponding to the conditions listed in Tables I and II are shown in Table III.

A. Second Order Zeeman Shift

The second order Zeeman shift of the clock transition due to a magnetic field induction B is [17]:

$$\Delta f_{2OZ} = 310.8\langle B^2\rangle \tag{2}$$

where the triangular brackets denote averaging over the ion cloud, B is expressed in units of 10^{-4} T and higher order terms have been neglected. Measurement of the frequency difference (the Larmor frequency) f_L between the $F = 0\, M_F = 0 \rightarrow F = 1\, M_F = 0$ and $F = 0\, M_F = 0 \rightarrow F = 1\, M_F = 1$ transitions yields a value for $|\langle B\rangle|$;

$$|\langle B\rangle| = \frac{f_L}{1.401 \times 10^6}, \tag{3}$$

where f_L is expressed in Hz. A complication arises [17] in that generally $\langle B^2\rangle \neq |\langle B\rangle|^2$. This introduces a further shift $\Delta f_{\text{M. Inh}}$, due to magnetic inhomogeneity, to the second order Zeeman shift, so that

$$\Delta f_{2OZ} = 310.8\left(\frac{f_L}{1.401 \times 10^6}\right)^2 + \Delta f_{\text{M. Inh}}. \tag{4}$$

The magnetic inhomogeneity shift $\Delta f_{\text{M. Inh}}$ is given by:

$$\Delta f_{\text{M. Inh}} = 310.8\left[\frac{\iiint_V n(x,y,z)|B(x,y,z)|^2 dx\, dy\, dz}{\iiint_V n(x,y,z) dx\, dy\, dz} - \left(\frac{\iiint_V n(x,y,z)|B(x,y,z)| dx\, dy\, dz}{\iiint_V n(x,y,z) dx\, dy\, dz}\right)^2\right] \tag{5}$$

where $n(x,y,z)$ is the spatially dependent number density of the ion cloud and the integrals are taken over the volume V of the ion cloud.

The spatial dependence of the magnetic induction, averaged over the ion cloud, was measured in IT-2 by monitoring the Larmor frequency as the ion cloud was displaced in the two transverse dimensions by DC biases applied to the trap RF electrodes. The dependence in longitudinal direction was then obtained from Maxwell's equations. A corresponding measurement was made using a Hall probe in both IT-1 and IT-2, with the vacuum systems opened. Although these measurements were made difficult by their limited spatial resolution, a comparison of their results in IT-2 was acceptably consistent.

We assume a cylindrical ion cloud whose axis is coincident with the longitudinal axis of the ion trap, with a radial density profile given by (A.7). The model of the ion cloud is discussed in more detail in the next section and in the Appendix. The measured magnetic inhomogeneities then result, using (5), in a calculated shift $\Delta f_{\text{M. Inh}} = 0.5 \pm 0.5$ mHz in both IT-1 and IT-2. The relatively large uncertainty in this shift reflects the fact that more work is needed to improve the characterization of the magnetic inhomogeneity.

The magnetic inhomogeneity shift was inadvertently overlooked in [12].

B. Second Order Doppler Shift

The second-order Doppler shift arises from the thermal motion of the ions, characterized by the temperature of the ion cloud, and the micro-motion of the ions at the frequency of the RF trap drive. Since the amplitude and consequently the velocity of the micro-motion increases away from the RF node along the longitudinal axis of the trap, a model of the radial density profile of the ion cloud is needed to calculate the resulting component of the second-order Doppler shift. Meis *et al.* [18] have presented a theoretical model of an ion cloud in a spherically symmetric potential in a hyperbolic Paul trap. In the Appendix, we present a corresponding model for a linear trap. In this and the next section we outline the use of this model, with some of the parameters in Table II, to calculate the radial density profile of the ion clouds (assumed to have cylindrical symmetry around the longitudinal trap axis) in IT-1 and IT-2, and consequently the second-order Doppler shift and the quadratic Stark shift in the two ion trap systems. The results of the calculations are presented in Table III.

The depth of the trap potential was calculated from a numerical model of the ponderomotive pseudo-potential of an infinitely long linear Paul trap, taking into account the finite diameter of the RF electrodes (Fig. 2). The depth depends on the geometry of the trap as well as frequency and voltage amplitude of the RF trap drive. Close to the axis of the trap the pseudo-potential is approximately harmonic in the transverse direction, and can be parameterized by ω_s, the transverse secular frequency of the empty trap (A.1). When ions are introduced into the trap the Coulomb repulsion between them modifies the potential seen by each ion, and the difference between the observed secular frequencies (Table II, Fig. 4) and theoretical value for an empty trap (Table III) reflect this change in the potential. The (Gaussian) radial density profile $n(r)$ (A.7) of the ion cloud was determined using the measured values of the temperature and the observed transverse secular frequency ω_m, as explained in the Appendix. The radius at which the density of the ion cloud falls to $1/e$ of its central density was simply calculated using the expression for $n(r)$, and the approximate number of ions in the cloud was obtained by integrating $2\pi r n(r)$ from $r = 0$ to infinity, and multiplying the result by the observed length of the ion cloud.

TABLE III

PARAMETERS CALCULATED FROM THE DATA IN TABLES I AND II ACCORDING TO A THEORETICAL MODEL OF THE ION CLOUD. THE VALUES GIVEN FOR THE NUMBER OF IONS IN THE TRAPS ARE ESTIMATES ONLY, BASED ON THE LINEAR ION DENSITY CALCULATED USING (A.4), AND THE OBSERVED LENGTH OF THE ION CLOUD IN TRAP 2.

	IT-1	IT-2
Trap potential well depth	1.2 eV	1.2 eV
Transverse secular frequency (empty trap)	23.5 kHz	22.4 kHz
Ion cloud radius (1/e of central density)	~ 1.9 mm	~ 1.8 mm
Ion number	$\sim 4 \times 10^5$	$\sim 2 \times 10^5$
Second-order Doppler shift	-9.3 ± 0.7 mHz	-8.5 ± 0.7 mHz
Stark shift	-0.13 ± 0.07 mHz	-0.11 ± 0.06 mHz

The component of the second-order Doppler shift due to the thermal motion of the ions is given by:

$$\left.\frac{\Delta f}{f}\right|_{\text{secular}} = -\frac{3}{2}\frac{kT}{mc^2} \tag{6}$$

where k is Boltzmann's constant, T is the kinetic temperature characterizing the secular motion of the ions, m is the mass of a $^{171}Yb^+$ ion and c is the speed of light.

The micro-motion contribution to the second order Doppler shift is calculated by averaging the shift over the profile of the cloud, with the result that the total second order Doppler shift is given by:

$$\left.\frac{\Delta f}{f}\right|_{\substack{\text{total}\\ \text{Second-order Doppler}}} = -\frac{3}{2}\frac{kT}{mc^2}\left(1+\frac{2}{3}\left(\frac{\omega_s}{\omega_m}\right)^2\right). \tag{7}$$

In the work described in this paper, the temperature of the ion cloud was calculated from the Doppler width of the optical transition driven by the 369 nm laser propagating along the longitudinal axis of the ion trap [5]. The temperature T_{long} so obtained characterizes the thermal secular motion of the ions in the longitudinal direction. It was found in a separate experiment, where the ion cloud temperature was measured similarly but with the laser propagating across the trap in the transverse direction, that the temperature T_{trans} characterizing the motion of the ions in the transverse direction is significantly higher (Fig. 7). For these transverse measurements, the laser was carefully aligned perpendicular to the z axis so that the temperature obtained was characteristic of the transverse secular motion only, and not the micro-motion at the 500 kHz RF drive frequency. The residual contribution of micro-motion in the direction of propagation of the laser beam, due to the finite width of the beam, was calculated to be less than 10 K. The discrepancy between the transverse and longitudinal temperatures is not surprising, at least qualitatively, when one considers that the heating of the ion cloud above the temperature (room temperature) of the He buffer gas occurs due to the purely transverse micro-motion of the ions. Although we have not studied the processes involved in detail, transfer of energy from the transverse degrees of freedom to the longitudinal appears to occur via Yb^+-Yb^+ Coulomb interactions, and more significantly at higher He pressures, via Yb^+-He collisions.

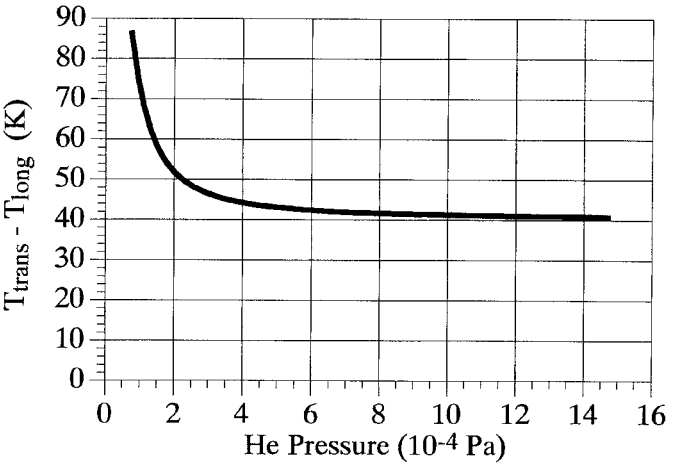

Fig. 7. Numerical fit to the measured difference between the ion cloud temperatures measured (see text) in the longitudinal and transverse directions, as a function of He pressure. The uncertainty in the measured difference is estimated to be less than 10 K.

Since the motional energy in each of the three spatial degrees of freedom of the ion cloud is not equal, the ion cloud is not in thermal equilibrium. The assumption of a Maxwellian velocity distribution made in the derivation of (7), and the precise meaning of transverse and longitudinal temperatures is therefore, to some extent, questionable and has not been studied in detail. Nevertheless, because, for the purposes of the present work, the temperature difference between the longitudinal and transverse degrees of freedom is approximately 60 K, which is significantly smaller than the temperature measured in the longitudinal direction ($\sim$ 360 K), we use as a best estimate of the second-order Doppler shift a modified version of (7):

$$\left.\frac{\Delta f}{f}\right|_{\substack{\text{total}\\ \text{Second-order Doppler}}} = -\frac{3}{2}\frac{k}{mc^2}\left(T_{\text{long}}+\frac{2}{3}T_{\text{trans}}\left(\frac{\omega_s}{\omega_m}\right)^2\right). \tag{8}$$

The uncertainties in the second order Doppler shifts given in Table III reflect only the uncertainties in the temperature and secular frequency measurements.

C. Quadratic Stark Shift

The quadratic Stark shift is given by:

$$\left.\frac{\Delta f}{f}\right|_{\text{Stark}} = -k_s\langle E^2\rangle \tag{9}$$

where the triangular brackets denote averaging of the square of the electric field amplitude E over a cycle of the RF trapping field and over the calculated density profile of the ion cloud. The experimentally determined value of k_s for $^{171}Yb^+$ is $2\pm1\times10^{-21}m^2V^{-2}$ [1]. The averaging over the radial density profile of the ion cloud is carried out using a similar method (see Appendix) to that used to obtain (7), with the result (A.12)

$$\left.\frac{\Delta f}{f}\right|_{\text{Stark}} = -4k_s\left(\frac{\omega_s}{\omega_m}\right)^2\frac{m\Omega^2}{q^2}kT_{\text{trans}}. \tag{10}$$

Here q is the electronic charge, $\Omega/2\pi$ is the frequency of the RF trap drive, and the temperature T_{trans} characterizing the transverse motion of the ions has been substituted for T in (A.12).

The value for k_s may also be used to calculate [17] the fractional frequency shift due to ambient blackbody radiation. The resulting fractional shift, approximately -1.4×10^{-15}, is presently negligible.

V. Final Value of the Clock Frequency

The corrections applied to the raw clock frequencies from the two ion trap systems, measured on the same day under operating conditions corresponding to Tables I–III, are detailed in Table IV.

It is evident that, despite the significantly different corrections for the second order Doppler shift applied to the raw frequency from each ion trap, the two final frequency values agree to within 3 parts in 10^{14}, although the uncertainties in the two values are somewhat larger.

We have made a number of measurements of the $^{171}Yb^+$ clock frequency over a period of more than 12 months. The results are shown in Fig. 8. Up to the date MJD 50139, the $^{171}Yb^+$ clock frequencies are corrected for the variation (averaged over 60 days), with respect to the SI second, of the frequency of the hydrogen maser used as the local reference. The data for the absolute hydrogen maser frequency variations since this date is not available at the time of writing, and the corresponding data points in Fig. 8 are corrected according to an extrapolation of the H maser frequency variation.

On three occasions the $^{171}Yb^+$ clock frequency was measured on IT-1 and IT-2 either simultaneously or on the same day. In each case, the agreement between the two frequencies is much better than 1 part in 10^{13}. During the period over which the data shown in Fig. 8 were obtained, both ion trap systems were dismantled and reassembled several times for various reasons, apparently without substantially affecting the corrected clock frequencies.

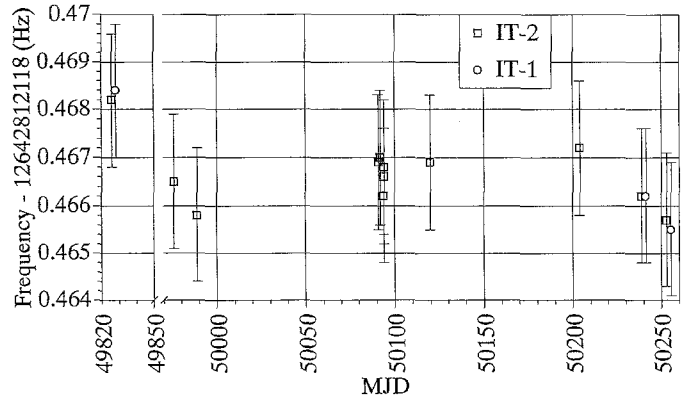

Fig. 8. Corrected $^{171}Yb^+$ clock frequencies measured over a period of approximately 14 months. MJD = Modified Julian Day, MJD 49820 = April 13 1995, MJD 50250 = 16 June 1996. On the three occasions (MJD 49826, 50239, and 50253) where determinations of the clock frequency were made using IT-1, the corresponding measurements on IT-2 were made simultaneously (on the first two occasions) or on the same day (third occasion). The data points are displaced horizontally on the plot for clarity. All of the data shown here were obtained with 10 V applied to the end electrodes, with the exception of the MJD 49826 data, where 20 V was used. Other trap parameters, such as He pressure, RF voltage and trap contents varied significantly between determinations. The data set taken on MJD 49826 was previously reported [12], and that taken on MJD 50253 is detailed in Tables I–IV in the present paper.

Much of the variation in the corrected clock frequencies since MJD 48950 can be explained by the day-to-day variation in the H maser frequency of a few parts in 10^{14}, resulting from nonoptimal auto-tuning of the masers NML-Maser 2 and NML-Maser 1. We cannot find evidence of a maser frequency variation of magnitude sufficient to explain the outlying data points obtained on MJD 49826. The reason for these outlying points is not known, although the two trap systems were still in good agreement on that date.

The uncertainties in the individual clock frequency determinations represented by the error bars on Fig. 8, and shown in Table IV, are largely statistical. The principal systematic errors in the clock frequency determinations will result from any inaccuracies in the model of the ion cloud, described in the Appendix, used to calculate the second-order Doppler shift. The two principal assumptions made in the derivation of (A.10) were first that the ion cloud is infinitely long, so that the distortion of the transverse ponderomotive pseudo-potential due to the presence of the end electrodes is neglected, and second that the potential seen by the trapped ions remains harmonic despite the distortion introduced by the space-charge of the ion cloud. Inclusion of the end electrodes and the space charge into the model of the ion cloud has not yet been attempted for the ion trap systems discussed in this paper, although some progress has been made on the space charge problem by Prestage *et al.* [19] for the case of a $^{199}Hg^+$ ion trap.

An experimental test of the validity of the present ion cloud model used to calculate the second-order Doppler shift, and also the relatively insignificant quadratic Stark

TABLE IV
CORRECTIONS APPLIED TO THE RAW CLOCK FREQUENCIES.

	IT-1	IT-2
Raw clock frequency	12642812119.2529 ± 0.0003 Hz	12642812119.2781 ± 0.0003 Hz
Corrections (measured directly)		
C field (2nd order Zeeman)	−0.7869 ± 0.0002 Hz	−0.8108 ± 0.0002 Hz
He pressure shift	−0.00038 ± 0.00015 Hz	−0.00058 ± 0.00015 Hz
Total measured corrections	−0.7873 ± 0.00025 Hz	−0.8114 ± 0.00025 Hz
Corrections (calculated according to model)		
Second order Doppler shift	0.0093 ± 0.0007 Hz	0.0085 ± 0.0007 Hz
Stark shift	0.00013 ± 0.00007 Hz	0.00011 ± 0.00006 Hz
Magnetic inhomogeneity shift	−0.0005 ± 0.0005 Hz	−0.0005 ± 0.0005 Hz
Total calculated corrections	0.0089 ± 0.00086 Hz	0.0081 ± 0.00086 Hz
Correction for reference maser rate vs TAI	−0.0091 ± 0.001 Hz	−0.0091 ± 0.001 Hz
Corrected clock frequency (vs TAI)	12642812118.4654 ± 0.0014 Hz	12642812118.4657 ± 0.0014 Hz

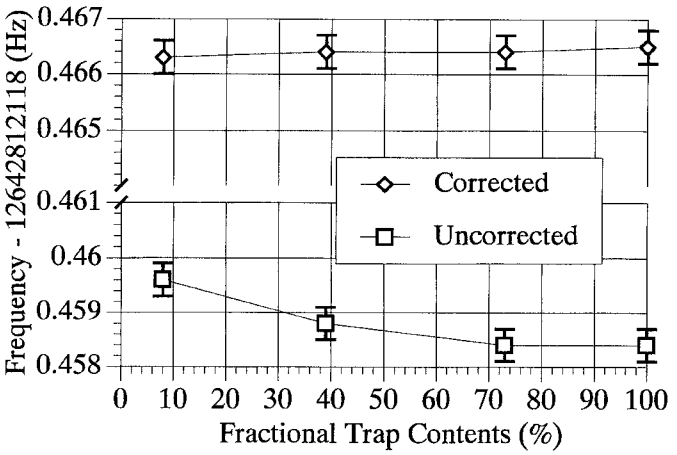

Fig. 9. Variation in the measured $^{171}Yb^{+}$ clock frequency, uncorrected and corrected using (8) and (10) for the varying second-order Doppler shift and (insignificantly small) quadratic Stark shift, as a function of the number of ions in the trap. A trap content of 100% corresponds to typical conditions under which the data shown in Fig. 8 was obtained. Both data sets are corrected for all the other shifts listed in Table IV. The end electrode voltage was 10 V. The error bars represent the statistical uncertainty in the raw clock frequencies only.

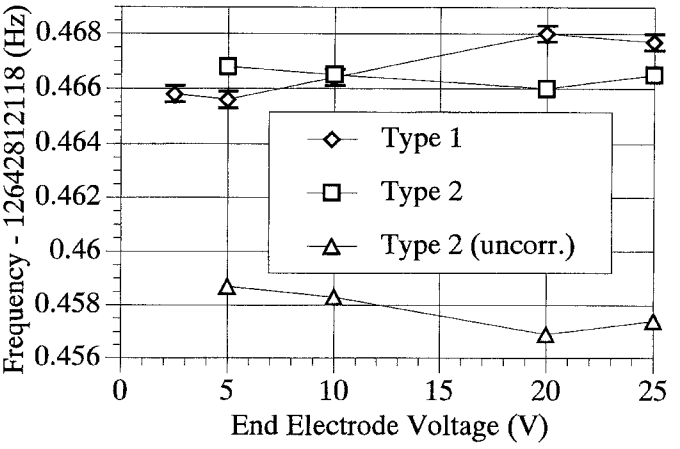

Fig. 10. Variation in the measured $^{171}Yb^{+}$ clock frequency as the voltage on the end electrodes was varied. Data is presented for two different shapes of end electrodes, shown in Fig. 11. The data sets are corrected for all the shifts listed in Table IV, except for one where the correction for the second-order Doppler shift and (insignificantly small) quadratic Stark shift have been removed. The error bars represent the statistical uncertainty in the raw clock frequencies only, and are shown on only one data set for clarity.

shift, should ideally involve making determinations of the corrected $^{171}Yb^{+}$ clock frequency while the ion trap systems are operated over a very wide range of conditions. Such an investigation has not been made, and indeed may be impractical due to the relatively limited range of operating parameters over which the ion trap systems will usefully operate as frequency standards. However, in this section, we present the results of a preliminary experimental investigation of the validity of the ion cloud model, where the trap contents have been varied, the voltage on the DC end electrodes (Fig. 2) has been varied and the shape of the end electrodes has been changed.

Fig. 9 shows the variation in the measured clock frequency observed as the number of ions in the trap was reduced in reproducible steps by grounding the end electrodes for a few microseconds at a time. The other trapping parameters were set to values similar to those shown in Table I. After the frequency measurements were made, the trap-loaded secular frequencies corresponding to each data point were measured, as were the ion cloud temperatures (which showed insignificant variation). It is evident that, after the corresponding corrections were made to the clock frequencies, the present model for the second-order Doppler shift adequately accounts for changes in the number of ions in the trap, and consequently the size of the ion cloud, over the range of values tested.

Fig. 10 shows an analogous set of data, but where the end electrode voltage was varied, with other trapping parameters set to values similar to those shown in Table I. A significant variation in the corrected clock frequencies is evident as the end electrode voltage is varied, indicating a partial breakdown of the model for the second-order Doppler shift. It was surmized that this might be due to the electric field from the relatively large end electrodes (type 1 electrodes, Fig. 11), used for most of the work described in this paper, distorting the cylindrical pondero-

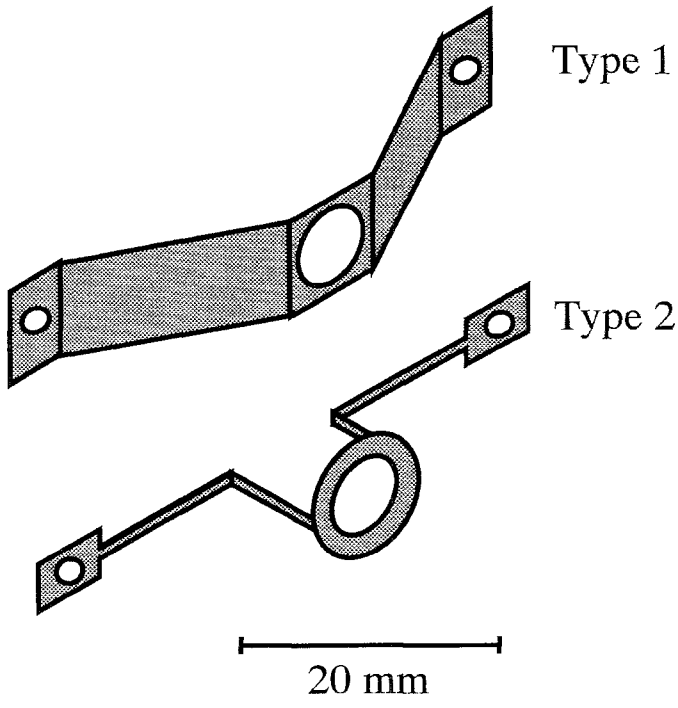

Fig. 11. Type 1 and type 2 end electrode shapes. The electrodes are mounted with the central hole coincident with the longitudinal axis of the ion trap (Fig. 1). The diameter of the central hole was the same (6 mm) for both types. Type 2 end electrodes were fitted to IT-2 for the data taken on MJD 49826 and MJD 50204 (see Fig. 8). All other data shown in Fig. 8 was taken with type 1 end electrodes fitted to both ion trap systems.

motive pseudo-potential. To test this theory, a set of end electrodes (type 2) which approximated more closely the case of a thin ring electrode around the longitudinal axis of the ion trap were installed in IT-2. The corresponding dependence (Fig. 10) of the corrected clock frequency on the end electrode voltage is weaker than with the type 1 electrodes, but still significant. Furthermore, when the dependence of the corrected clock frequency on the number of ions in the trap is measured using the type 2 electrodes (the data in Fig. 9 was taken using type 1 end electrodes), a variation in the corrected clock frequency of up to ± 1 mHz was observed. Consequently, from our measurements to date, we estimate the systematic uncertainty due to the validity of the model of the ion cloud used to calculate the second-order Doppler shift to be ± 1.5 mHz.

The corrected clock frequencies obtained with the type 1 and type 2 end electrodes agree for an end electrode voltage of 10 V, consequently only data taken under this condition is included in the calculation of our best estimate of the $^{171}Yb^{+}$ clock frequency.

The possibility of contamination of the helium buffer gas affecting the measured frequency of the $^{171}Yb^{+}$ clock transition was also investigated. For all of the data reported in this paper, helium at the required pressures was introduced into the vacuum systems of IT-1 and IT-2 through a heated quartz membrane. On IT-1, a glass flask of spectroscopic grade helium is also connected through a sapphire leak valve, and helium from this source can reasonably be expected to have different levels and types of contaminants compared with helium obtained from the quartz membrane. When an equal pressure of helium was obtained from the glass flask, rather than from the quartz membrane, the measured clock frequency of IT-1 changed by less than 0.1 mHz, indicating that at the present level of accuracy, contamination of the helium used as a buffer gas is probably not significant.

We do not expect a significant frequency shift due to any residual first-order Doppler effect resulting from curvature of the microwave wavefronts. This would to a very good approximation contribute a broadening (which we have not observed), rather than a shift, in the microwave resonance because of the cyclic nature of the ions motion in the trap.

Discarding the MJD 49826 data, the mean of the $^{171}Yb^{+}$ clock frequency measurements shown in Fig. 8 is 12 642 812 118.4662 Hz, with a standard deviation of 0.00054 Hz, and a calculated statistical uncertainty table (4) of ± 1.4 mHz in each determination. Consequently, we estimate our total uncertainty in Hz as $((0.0014(\text{stat}))^2 + (0.0015(\text{syst}))^2)^{1/2} = \pm 0.002$ Hz, yielding our best estimate for the $^{171}Yb^{+}$ clock frequency 12 642 812 118.466 $\pm$ 0.002 Hz.

Our measurement of the clock frequency is in agreement with that of Tamm *et al.* [1], 12 642 812 118.471$\pm$0.009 Hz.

VI. Conclusion

We have measured the frequency of the $^{171}Yb^{+}$ 12.6 GHz $M_F = 0 \rightarrow 0$ ground state hyperfine "clock" transition in buffer gas-cooled ion clouds confined in two similar, but not identical, linear Paul traps. After correction for the known differences between the two ion traps, including significantly different second-order Doppler shifts, the frequencies have agreed on each occasion on which they were measured within ± 3 parts in 10^{14}.

Measurements taken over a period of more than 12 months yield a value for the frequency of the 12.6 GHz $M_F = 0 \rightarrow 0$ clock transition in an isolated $^{171}Yb^{+}$ ion at zero temperature, velocity, electric field, and magnetic field, of 12 642 812 118.466 $\pm$ 0.002 Hz. An experimental investigation of the validity of the model used to calculate the second-order Doppler shift experienced by the ions shows that the model is probably valid under the present range of operating parameters to within ± 1.5 mHz.

Acknowledgment

The authors thank Dr. A. G. Mann and Dr. D. G. Blair of the Department of Physics, University of Western Australia, for the loan of the cryogenic sapphire resonator on which our microwave system is based.

APPENDIX
CALCULATION OF THE SECOND-ORDER DOPPLER SHIFT

The calculation presented here of the second order Doppler shift for a linear ion trap is an extension to the linear ion trap case of previous work [18] on a spherically symmetric potential in a hyperbolic Paul trap.

The ponderomotive trapping pseudo-potential experienced by an ion of mass m close to the longitudinal axis of an infinitely long linear Paul trap can be written in the form:

$$\Psi(r) = \frac{m\omega_s^2 r^2}{2} \tag{A.1}$$

where $\omega_s/2\pi$ is the transverse secular frequency and r is the distance from the longitudinal axis of the trap. In the limit where the radius r_e of the RF electrodes is small compared with their separation a, the expression for ω_s is [20]:

$$\omega_s = \frac{4eV_0}{\sqrt{2}m\Omega a^2 \ln\left(\frac{a}{r_e}\right)} \tag{A.2}$$

where V_0 is the peak voltage on the RF electrodes and $\Omega/2\pi$ is the frequency of the RF field.

Since the RF cycle average of the energy associated with the ponderomotive pseudo-potential is equal to the RF cycle average of the kinetic energy of the micro-motion of the ions, given by $m\langle v^2\rangle/2$, the second-order Doppler shift due to the micro motion is given by:

$$\begin{aligned}\left.\frac{\Delta f(r)}{f}\right|_{\text{micro}} &= -\frac{1}{2}\frac{\langle v^2\rangle}{c^2} \\ &= -\frac{\Psi(r)}{mc^2}. \\ &= -\frac{\omega_s^2 r^2}{2c^2}\end{aligned} \tag{A.3}$$

To determine the total second-order Doppler shift due to the micro-motion, (A.3) must be integrated over the density profile of the ion cloud. The spatial distribution of the ion density in the cloud at a temperature T, assuming a Maxwellian distribution, is given by [21]:

$$n(r) = C\exp\left(\frac{-V(r)}{kT}\right) \tag{A.4}$$

where C is a normalization constant. $V(r)$ is the total radial potential seen by the ion, given by:

$$\begin{aligned}V(r) &= \frac{m\omega_s^2 r^2}{2} + \Phi(r) \\ &= \frac{m\omega_m^2(r) r^2}{2} + \Phi(0)\end{aligned} \tag{A.5}$$

where $\Phi(r)$ is the space charge potential due to the other ions in the trap and $\omega_m(r)/2\pi$ is the loaded-trap secular frequency, in which the radial dependence of $\Phi(r)$ has been included. If the potential is assumed to remain harmonic in the presence of the space charge, $\omega_m(r)$ may be approximated by the constant value ω_m, so that

$$V(r) = \frac{m\omega_m^2 r^2}{2} + \Phi(0). \tag{A.6}$$

A numerical solution for the spatial distribution of the ion cloud, taking account of space-charge, indicates that the effective potential $\Phi(r)$ deviates from harmonicity by less than 10% over the radius of the ion cloud under the conditions of the present work.

An expression for the ion density is obtained by substituting (A.6) into (A.4),

$$n(r) = C'\exp\left(\frac{-m\omega_m^2 r^2}{2kT}\right). \tag{A.7}$$

The second-order Doppler shift due to the micro-motion is then obtained using (A.7) and (A.3) and integrating over the ion cloud

$$\begin{aligned}\left.\frac{\Delta f}{f}\right|_{\text{micro}} &= -\left(\frac{\omega_s^2}{2c^2}\right)\frac{\int_0^\infty 2\pi r\, r^2 n(r)dr}{\int_0^\infty 2\pi r\, n(r)dr} \\ &= -\frac{kT}{mc^2}\left(\frac{\omega_s}{\omega_m}\right)^2.\end{aligned} \tag{A.8}$$

The second-order Doppler shift due to the secular motion is given by:

$$\left.\frac{\Delta f}{f}\right|_{\text{secular}} = -\frac{3}{2}\frac{kT}{mc^2}, \tag{A.9}$$

and the total second-order Doppler shift is then

$$\left.\frac{\Delta f}{f}\right|_{\substack{\text{total}\\ \text{Second-order Doppler}}} = -\frac{3}{2}\frac{kT}{mc^2}\left(1 + \frac{2}{3}\left(\frac{\omega_s}{\omega_m}\right)^2\right). \tag{A.10}$$

This result is identical to that of Meis *et al.* [18] for a spherically symmetric potential in a hyperbolic Paul trap.

The expression for the quadratic Stark shift (10) was obtained from (9) by noting that the square of the RF electric field amplitude averaged over one cycle in a cylindrical harmonic ponderomotive pseudo-potential characterized by an empty trap secular frequency ω_s is given by:

$$E^2(r) = 2\left(\frac{\omega_s m\Omega r}{q}\right)^2 \tag{A.11}$$

where q is the electronic charge. The quadratic Stark shift, averaged over the ion cloud is then obtained using (9)

$$\begin{aligned}\left.\frac{\Delta f}{f}\right|_{\text{Stark}} &= -2k_s\left(\frac{\omega_s m\Omega}{q}\right)^2\frac{\int_0^\infty 2\pi r\, r^2 n(r)dr}{\int_0^\infty 2\pi r\, n(r)dr} \\ &= -4k_s\left(\frac{\omega_s}{\omega_m}\right)^2\frac{m\Omega^2}{q^2}kT.\end{aligned} \tag{A.12}$$

References

[1] C. Tamm, D. Schnier, and A. Bauch, "Radio-frequency laser double-resonance spectroscopy of trapped ^{171}Yb ions and determination of line shifts of the ground-state hyperfine resonance," *Appl. Phys. B, Photophys. Laser Chem.*, vol. 60, pp. 19–29, 1995.

[2] R. L. Tjoelker, J. D. Prestage, G. J. Dick, and L. Maleki, "Recent stability comparisons with the JPL linear trapped ion frequency standards," in *Proc. 48th Annu. IEEE 1994 Int. Freq. Contr. Symp.*, Boston, MA, pp. 739–743.

[3] R. L. Tjoelker, J. G. Prestage, G. J. Dick, and L. Maleki, "Long term stability of Hg^+ trapped ion frequency standards," in *Proc. 47th Annu. IEEE Int. Symp. Freq. Contr.*, Salt Lake City, UT, 1993, p. 132.

[4] D. J. Seidel and L. Maleki, "Progress toward the development of a ytterbium ion standard," in *Proc. IEEE 1994 Int. Freq. Contr. Symp.*, Boston, MA, pp. 761–768.

[5] P. T. H. Fisk, M. J. Sellars, M. A. Lawn, and C. Coles, "Performance of a microwave frequency standard based on laser-detected, trapped $^{171}Yb^+$ ions," *Appl. Phys. B, Photophys. Laser Chem.*, vol. 60, pp. 519–527, 1995.

[6] P. T. H. Fisk, M. J. Sellars, M. A. Lawn, C. Coles, A. G. Mann, and D. G. Blair, "Performance of a prototype microwave frequency standard based on trapped $^{171}Yb^+$ ions," in *Proc. 48th Annu. IEEE Int. Symp. Freq. Contr*, Boston, MA, 1994, pp. 139–143.

[7] A. Bauch, D. Schnier, and C. Tamm, "Frequency measurement of the hyperfine splitting of $^{171}Yb^+$ ions stored in a Paul trap," in *Proc. 7th European Freq. Time Forum*, Neuchâtel, Switzerland, 1993.

[8] D. J. Seidel, A. Williams, R. W. Berends, and L. Maleki, "The development of a ytterbium ion frequency standard," in *Proc. 46th Annu. IEEE Int. Freq. Contr. Symp.*, 1992, p. 70.

[9] R. Casdorff, V. Enders, R. Blatt, W. Neuhauser, and P. E. Toschek, "A 12 GHz standard clock on trapped ytterbium ions," *Annalender Physik*, vol. 48, no. 7, p. 41, 1991.

[10] L. S. Cutler, R. P. Giffard, and M. D. McGuire, "Thermalization of ^{199}Hg ion macromotion by a light background gas in an RF quadrupole trap," *Appl. Phys. B, Photophys. Laser Chem.*, vol. 36, pp. 137–142, 1985.

[11] J. D. Prestage, G. J. Dick, and L. Maleki, "New ion trap for frequency standard applications," *J. Appl. Phys.*, vol. 66, no. 3, p. 1013, Aug., 1989.

[12] M. J. Sellars, P. T. H. Fisk, M. A. Lawn, and C. Coles, "Further investigation of a prototype microwave frequency standard based on trapped $^{171}Yb^+$ ions," in *Proc. 49th Annu. IEEE Int. Symp. Freq. Contr.*, San Francisco, CA, 1995, pp. 66–73.

[13] P. T. H. Fisk, M. A. Lawn, and C. Coles, "Laser cooling of $^{171}Yb^+$ ions in a linear Paul trap," *Appl. Phys. B, Photophys. Laser Chem.*, vol. B57, 1993, p. 287.

[14] P. T. H. Fisk, M. A. Lawn, and C. Coles, "Progress at CSIRO Australia towards a microwave frequency standard based on trapped, laser-cooled $^{171}Yb^+$ ions," in *Proc. 47th Annu. IEEE Int. Freq. Contr. Symp.*, Salt Lake City, UT, 1993, p. 139.

[15] A. J. Giles, A. G. Mann, S. K. Jones, D. G. Blair, and M. J. Buckingham, "A very high stability sapphire-loaded superconducting cavity oscillator," *Physica B Condensed Matter*, vol. 145, no. 1, pp. 165-166, Aug., 1990.

[16] D. J. Wineland, W. M. Itano, J. C. Bergquist, J. J. Bollinger, F. Diedrich, and S. L. Gilbert, "High accuracy spectroscopy of stored ions," in *Frequency Standards and Metrology*, ed. A. D. Marchi, Springer-Verlag, Berlin, 1989, pp. 71–77.

[17] J. Vanier and C. Audoin, *The Quantum Physics of Atomic Frequency Standards*. Adam Hilger, Bristol, U.K., 1989.

[18] C. Meis, M. Desaintfuscien, and M. Jardino, "Analytical calculation of the space charge potential and the temperature of stored ions in an RF quadrupole trap," *Appl. Phys. B, Photophys. Laser Chem.*, vol. 45, 1998, pp. 59–64.

[19] J. D. Prestage, R. L. Tjoelker, G. J. Dick, and L. Maleki, "Doppler sideband spectra for ions in a linear Paul trap," in *Proc. IEEE 1993 Int. Freq. Contr. Symp.*, Salt Lake City, UT, pp. 148–153.

[20] G. R. Janik, J. D. Prestage, and L. Maleki, "Simple analytic potentials for linear ion traps," *J. Appl. Phys.*, vol. 67, no. 10, pp. 6050–6055, 1990.

[21] L. S. Cutler, C. A. Flory, R. P. Giffard, and M. D. McGuire, "Doppler effects due to thermal macromotion of ions in an RF quadrupole trap," *Appl. Phys. B, Photophys. Laser Chem.*, vol. 39, pp. 251–259, 1986.

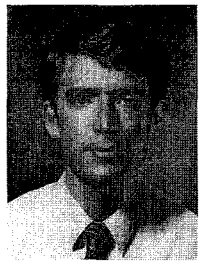

Peter Fisk was born in Kuala Lumpur, Malaysia, in 1959. He received the B.Sc. (Hons) degree in physics in 1982 and a Ph.D. degree in 1986, both from the Australian National University in Canberra, ACT, Autralia. His doctoral studies were in high resolution atomic laser spectroscopy at the Australian National University. He joined the CSIRO National Measurement Laboratory in Sydney, New South Wales, Australia to start and lead their trapped ion frequency standard project. Since 1993 he has been head of the Time and Frequency section in that organization.

Matthew Sellars was born in Canberra, ACT, Australia, in 1965. He received the B.Sc. degree in 1988, and the Ph.D. degree in 1996 from the Australian National University. He did his postgraduate research at the Australian National University in the field of high resolution laser spectroscopy of rare earth doped crystals. In 1994, he joined the Time and Frequency section of the National Measurement Laboratory, Sydney, New South Wales, Australia, as a postdoctoral fellow.

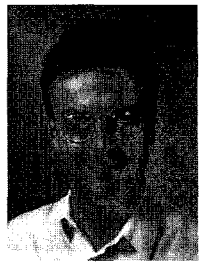

Malcolm Lawn was born in Melbourne, Victoria, Australia, in 1966. He received the B.App.Sc. degree in 1988 and the M.App.Sc. degree in thin-film technology in 1994, both from the Royal Melbourne Institute of Technology. From 1988 to 1990, he was a Research Assistant with the UV Photoelectron Spectroscopy Group at La Trobe University, Melbourne. In 1991 he joined the Time and Frequency Section, CSIRO National Measurement Laboratory, Sydney, New South Wales, Australia, as a Staff Scientist.

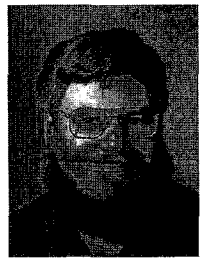

Colin Coles was born in Sydney, New South Wales, Australia, in 1953. After a 16-year career in satellite and radio communications and precision timekeeping, in 1991 he joined the Time and Frequency Section of the CSIRO National Measurement Laboratory, Sydney, New South Wales, Australia, as an electronics and microwave engineer.